Direct comparison of phase-sensitive vibrational sum frequency generation with maximum entropy method: Case study of water

Alex G. F. de Beer,[1] Jean-Sebastièn Samson,[1] Wei Hua,[2] Zishuai Huang,[2] Xiangke Chen,[2] Heather C. Allen,[2] and Sylvie Roke[3,a)]

[1]*Max Planck Institute for Intelligent Systems (formerly Max Planck Institute for Metals Research), Heisenbergstrasse 3, D70569 Stuttgart, Germany*

[2]*Department of Chemistry, The Ohio State University, 100 West 18th Avenue, 43210 Columbus, Ohio, USA*

[3]*Laboratory for Fundamental BioPhotonics (LBP), Institute of Bioengineering (IBI), École Polytechnique Fédérale Lausanne (EPFL), Station 17, CH-1015 Lausanne, Switzerland*

(Received 1 April 2011; accepted 19 October 2011; published online 8 December 2011)

We present a direct comparison of phase sensitive sum-frequency generation experiments with phase reconstruction obtained by the maximum entropy method. We show that both methods lead to the same complex spectrum. Furthermore, we discuss the strengths and weaknesses of each of these methods, analyzing possible sources of experimental and analytical errors. A simulation program for maximum entropy phase reconstruction is available at: http://lbp.epfl.ch/. © *2011 American Institute of Physics*. [doi:10.1063/1.3662469]

I. INTRODUCTION

Sum frequency generation (SFG) (Refs. 1–18) is a powerful technique for probing interfaces at the molecular level. Sum frequency (SF) photons can be generated when two laser pulses are spatially and temporally overlapped in a sample and induce a simultaneous infrared (IR) and Raman transition. Due to the symmetry requirements of this process, which is forbidden under the inversion symmetry found in many bulk materials and most liquids, SFG is inherently interface-selective. SFG has been successful in elucidating the molecular surface structure of many aqueous[12,19–24] and biologically relevant[23,25–35] systems.

Despite the success of SFG spectroscopy, there is an ongoing discussion about the interpretation of experimental findings on neat water/vapor interfaces[12,22,36–41] and at water in contact with phospholipid monolayers.[32,41–44] The main reason for this is that the evaluation of SFG intensity spectra is often non-straightforward: the SFG signal is proportional to the square of the nonlinear surface susceptibility $|\chi^{(2)}|^2$ or effective particle susceptibility $|\Gamma^{(2)}|^2$. As a result, interference between peaks gives rise to intensity cross terms, and interference between resonances and a weakly dispersed background may lead to line shapes that are hard to interpret. Furthermore, most aqueous systems consist of a superposition of vibrational resonances that form broad spectral features. These features cannot readily be assigned to distinct resonances, which has led to different interpretations of the structure of the water/vapor interface,[12,22,23,36–41] and of the structure of water in biologically relevant environments.[32,41–44]

Recently, however, two methods have been applied that provide additional information on surface structure in the form of a spectrum that is proportional to $\mathrm{Im}[\chi^{(2)}]$ rather than $|\chi^{(2)}|^2$. Phase-sensitive SFG (PS-SFG) (Refs. 35, 36, 39, 45–48) was introduced as a method to retrieve the complex nonlinear susceptibility. In PS-SFG interference between a measured signal and a reference provides a method to recover the complex SF spectrum of a planar surface. The resulting $\mathrm{Im}[\chi^{(2)}]$ response is a linear superposition of resonances. Furthermore, the sign of each resonance can be determined, which yields information on the absolute orientation of the transition dipole of molecules at an interface.

An alternative to PS-SFG is the maximum entropy method (MEM).[32] MEM is a computational method that retrieves complex data from an intensity spectrum. The maximum entropy method is widely used in geophysics,[49] economics,[50] and spectroscopy[51–53] and has been successfully applied to nonlinear microscopy[54] and coherent anti-stokes Raman spectroscopy[55–57] and recently, SFG spectroscopy.[32,44,58,59] Since MEM analysis is applied directly to intensity spectra, it can be a suitable alternative in cases where PS-SFG is not practical. In the case of sum frequency scattering,[33,60–68] for instance, a large number of scatterers contribute to the SFG signal. The positions of these scatterers are random; the overall detected intensity is an incoherent sum over all scatterers.[69] Since interferometric detection depends on reproducibility of the light path length of the SFG signal, it is not possible to gain a phase sensitive signal for randomly distributed scatterers. MEM analysis, on the other hand can be performed on a regular intensity spectrum, without the need for an interferometric measurement, so that the method can be applied to any case in which a non-interferometric intensity spectrum is available.

At first glance, MEM analysis seems to accomplish the impossible: since intensity spectra are proportional to the absolute square of $\chi^{(2)}$ or $\Gamma^{(2)}$, all phase information is deemed lost. Since the underlying data consist of a collection of resonances, however, a MEM algorithm can recover complex data by using the fact that all of these resonances must be decaying in time, rather than growing or staying constant in time.

MEM analysis was first applied to SFG spectroscopy in an investigation of phospholipid monolayers on water.[34]

a)Author to whom correspondence should be addressed. Electronic mail: sylvie.roke@epfl.ch.

The results of this study were later questioned on the basis of a difference between the MEM result and results obtained by molecular dynamics simulations[43] and PS-SFG measurements.[35,41] However, The discrepancies between MEM analysis and PS-SFG measurements could be explained.[44]

In this article, we investigate to what extent the complex signal retrieved from a MEM analysis corresponds to the signal obtained in a phase sensitive SFG measurement. We present the theoretical background of both methods, and show that PS-SFG and MEM are analogous: the experimental procedure of PS-SFG is mirrored in the theoretical calculation of the MEM algorithm. We offer insight into the working of the MEM algorithm and discuss which assumptions are needed to retrieve a complex phase from an intensity spectrum. We then compare experimental results obtained from PS-SFG to results obtained when the MEM algorithm is applied to the intensity spectrum of the same recording. We show that whenever PS-SFG detection is not possible due to practical limitations, MEM analysis provides a reconstruction of the relative phase of each data point in an intensity spectrum. Moreover, when a suitable criterion is found for retrieving the error phase, it is possible to recover a full complex spectrum, without the need for a phase sensitive measurement. Finally, we discuss the possible experimental and computational distortions of complex SFG spectra that may occur in PS-SFG and MEM analysis.

II. PHASE SENSITIVE MEASUREMENTS AND PHASE RETRIEVAL

The reflected SFG response of a planar interface is typically described in terms of a nonlinear surface polarization $\mathbf{P}^{(2)}$, which acts as the source term of the SFG field. The interaction of the (local) source fields $\mathbf{E}_1$ and $\mathbf{E}_2$ with the nonlinear susceptibility tensor $\boldsymbol{\chi}^{(2)}$ determines the strength and direction of $\mathbf{P}^{(2)}$ according to

$$P^{(2)}_{0,i} = \epsilon_0 \chi^{(2)}_{ijk} E_{1,j} E_{2,k}. \tag{1}$$

We assume a time variation of $\exp(i\omega t)$ at frequency ω for all fields. The nonlinear surface polarization acts as the source of the sum-frequency field, so that the eventual signal intensity I_{SFG} becomes

$$I_{SFG} \propto |\mathbf{u}_0 \cdot \mathbf{P}^{(2)}|^2 \propto |\boldsymbol{\chi}^{(2)}|^2, \tag{2}$$

where $\mathbf{u}_0$ is the (local) polarization direction of the sum-frequency field. The nonlinear susceptibility $\boldsymbol{\chi}^{(2)}$ holds information on molecular density, composition, and orientation of the infrared transition dipole. For most compounds, $\boldsymbol{\chi}^{(2)}$ can be described with a superposition of a non-resonant background and a number of resonances:

$$\boldsymbol{\chi}^{(2)} = A_{NR} e^{i\phi_{NR}} + \sum_n \frac{A_{R,n}}{\omega - \omega_{0,n} - i\Upsilon_n}, \tag{3}$$

where A_{NR} is the non-resonant amplitude, and ϕ_{NR} is the phase difference between non-resonant background and resonances. $A_{R,n}$ is the resonant amplitude of the nth resonance, with central frequency $\omega_{0,n}$, and line width (half width at half maximum) Υ_n. In the time domain, the resonance at frequency $\omega_{0,n}$ represents an oscillation with the same frequency. The line width Υ_n is the decay rate of this resonance, so that the oscillation, in the time domain, is given by $\exp[i(\omega_{0,n} + i\Upsilon_n)t] = \exp[i\omega_{0,n}t]\exp[-\Upsilon_n t]$. Alternatively, the pair of resonance frequency $\omega_{0,n}$ and line width Υ_n can be interpreted as a complex resonance frequency with real part frequency and imaginary part line width: in the time domain the resonance is an exponentially decaying oscillator, i.e., $\Upsilon_n > 0$. Although ω in Eq. (3) can only (physically) attain real values, mathematically speaking Eq. (3) contains poles (i.e., $\boldsymbol{\chi}^{(2)}$ is infinite) at the positions of the complex resonance frequencies.

A. Phase sensitive SFG

In a reflection mode SFG experiment, the recorded quantity is the frequency or time domain intensity, so that the detection is limited to the absolute square $|\boldsymbol{\chi}^{(2)}|^2$ of the nonlinear susceptibility. Because of the interference between resonances and non-resonant background, retrieval of resonance peak positions and amplitudes is often complicated. Moreover, the sign of a resonance is often hard to determine unambiguously for the same reason. In order to alleviate these limitations, PS-SFG was introduced.[36,39,45–47]

In a PS-SFG experiment, two sum-frequency fields are mixed: a signal from a sample, and that of a local oscillator (LO). The mixing of the sum-frequency fields of the sample and the LO causes an interference pattern in the intensity spectrum. This interference pattern is compared to that of a second measurement, in which the sum-frequency field of the LO is mixed with that of a reference of which the complex $\boldsymbol{\chi}^{(2)}$ is known. Figure 1(a) shows the PS-SFG setup as introduced by Nihonyanagi *et al.*:[39] a fs IR pulse and a ps visible beam are spatially and temporally overlapped on a sample. The reflected beams as well as the generated SFG signal are collected by a parabolic mirror and refocused on a crystal surface acting as the LO. A time delay of several ps is introduced in the primary SFG signal by a thin silica window (not shown), so that the SFG signal from sample and local oscillator are offset temporally. At the detector, the two SFG signals are dispersed by a grating. This dispersing also causes a stretching in time of the SFG pulses, so that they now overlap and interfere. The interference pattern in the frequency domain recorded by the detector is given by

$$\begin{aligned} I_{\mathrm{SFG}}(\omega) &= |E_{sample/ref} + E_{LO}|^2, \\ &= |E_{sample/ref}|^2 + |E_{LO}|^2 \\ &\quad + 2\mathrm{Re}[E_{sample/ref} E^*_{LO} e^{i\omega T}]. \end{aligned} \tag{4}$$

Here, $E_{sample/ref}$ and E_{LO} are the sample (or reference) and the LO SFG fields, respectively. T is the temporal delay between the sample and the LO fields. This delay is introduced experimentally, e.g., by passing the LO field through a silica window. Figure 1(c) shows a simulated example of the spectrum thus recorded, along with its computed Fourier transform. Since the cross terms $E_{sample} E^*_{LO} \exp(i\omega T)$ are temporally offset, they appear as side lobes in the Fourier transform. A single side lobe can be isolated computationally

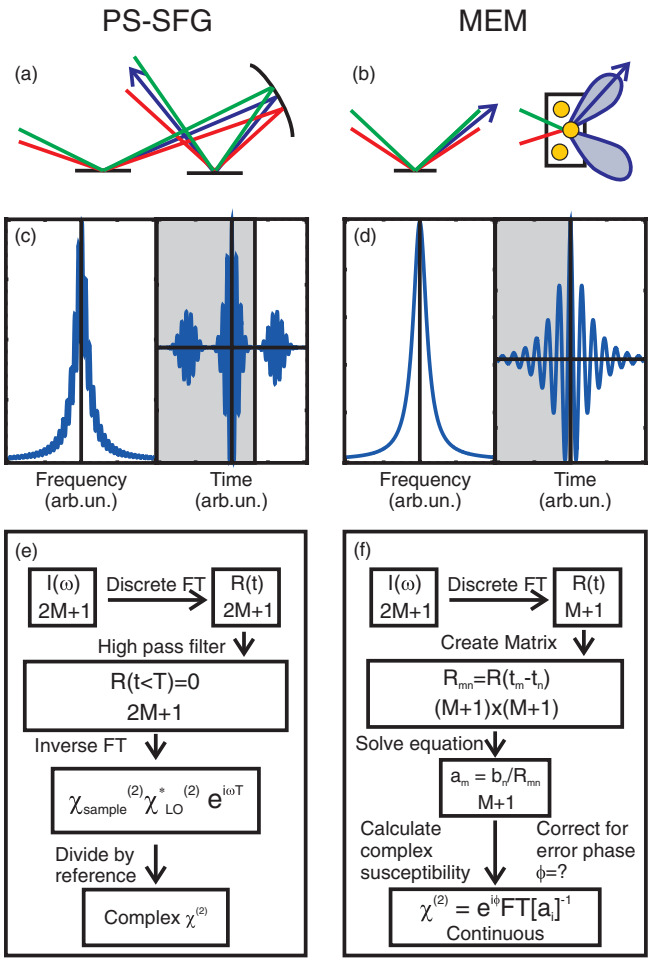

FIG. 1. Comparison between PS-SFG and MEM analysis. (a) Cartoon of a PS-SFG experimental setup. (b) Cartoon of regular reflection mode (left) and scattering mode (right) SFG setups. (c) Illustration of the relation between spectrum I(ω) and autocorrelation $R(t)$ in a PS-SFG measurement. (d) Idem for MEM analysis. (e) Flow chart for PS-SFG data analysis. (f) Flow chart for the maximum entropy method algorithm. 2M + 1 indicates the number of data points in the frequency domain spectrum.

by applying a high pass step filter (rejecting autocorrelation points within the gray area) and applying the inverse Fourier transform. This is shown in the flow scheme of Fig. 1(e). Finally, we can retrieve the nonlinear susceptibility $\boldsymbol{\chi}^{(2)}$ relative to that of the reference by dividing the filtered sample intensity by the filtered reference intensity:

$$\frac{\chi^{(2)}_{sample}}{\chi^{(2)}_{ref}} = \frac{C_{sample}}{C_{ref}} \frac{E_{sample}(\omega) E^*_{LO} e^{i\omega T}}{E_{ref}(\omega) E^*_{LO} e^{i\omega T}}, \quad (5)$$

$$= \frac{C_{sample}}{C_{ref}} \frac{E_{sample}(\omega)}{E_{ref}(\omega)},$$

where C_{sample} and C_{ref} are experimental corrections for reflectivity ratios and Fresnel factors (see Refs. 36, 39, 45–47). The result is a complex-valued expression, the imaginary part of which corresponds to Im[$\boldsymbol{\chi}^{(2)}$]. Im[$\boldsymbol{\chi}^{(2)}$] is a linear superposition of the resonances in $\boldsymbol{\chi}^{(2)}$:

$$\mathrm{Im}[\chi^{(2)}] = A_{NR} \sin\phi_{NR} - \sum \frac{A_{R,n}\Upsilon_n}{(\omega - \omega_{0,n})^2 + \Upsilon_n^2}. \quad (6)$$

It is convenient to know the value of Im[$\boldsymbol{\chi}^{(2)}$] for several reasons. First, since Im[$\boldsymbol{\chi}^{(2)}$] is a linear superposition of resonances, identifying a vibrational mode becomes more straightforward, since all cross terms have been eliminated. Second, $A_{R,n}$ is determined by the IR transition dipole and the Raman transition polarizability of a molecule, as well as its orientation. As such, the sign of of $A_{R,n}$ contains information on the absolute orientation of the transition dipole of a molecule with respect to the interface normal. If a reference sample with a known sign of $\boldsymbol{\chi}^{(2)}_{ref}$ is used and the spectral assignment of a line in a spectrum is known, the sign of Im[$\boldsymbol{\chi}^{(2)}$] yields exact information on the orientation (up or down with respect to the interface normal) of a molecule.

B. Maximum entropy analysis

The maximum entropy method provides a method for retrieving a complex spectrum from a bare intensity measurement. At first glance, this premise seems paradoxical, since an infinite number of reconstructions are possible for any given intensity spectrum. The paradox can be solved by imposing two requirements: (1) all the resonances that are present in a spectrum are exponentially decaying resonances and (2) all the information is contained within the spectrum. The first of these holds in general, due to conservation of energy, while the second one requires that a spectrum consists at most of resonances that are lying within the observation window and a constant background. When the above requirements are met, a single solution exists that provides the relative phase of all points in a spectrum.[70] Thus, the problem of finding the phase for every point in the spectrum is reduced to finding the phase for the overall spectrum.

MEM analysis can be applied to SFG intensity measurements.[32,44] Two of the possible experimental configurations are shown in Fig. 1(b): a reflection mode experiment (left) and a scattering mode experiment (right). In both cases, an IR and visible pulse are spatio-temporally overlapped on a sample. The reflected (scattered) SF signal is then collected and recorded.

MEM analysis was originally developed[70] to extend autocorrelations beyond a cutoff time T_{max}. The underlying concept is shown in Fig. 1(d): an intensity spectrum (left) showing a number of resonances consists of 2M + 1 data points measured at a frequency interval $\Delta\omega$. In order to be suitable for MEM analysis, intensity spectra must be corrected for laser power and any baseline offsets must be removed. The Fourier transform of the spectrum yields the autocorrelation function $R(t)$ (right), which shows the exponentially decaying resonances present in the spectrum. Since for an intensity spectrum $R(-t) = R^*(t)$, we may take only positive autocorrelation values (i.e., for which $t \geq 0$, which lie outside of the gray area in Fig. 1(d)). The limited spectral resolution $\Delta\omega$ cuts off the autocorrelation function at a time $T_{max} = 2\pi/(\Delta\omega)$.

Beyond the time point T_{max}, no information is available, so that a prediction of values is necessary. The obvious choice – to pad the autocorrelation with zeros – induces ringing artifacts in the frequency domain. If we assume, however, that

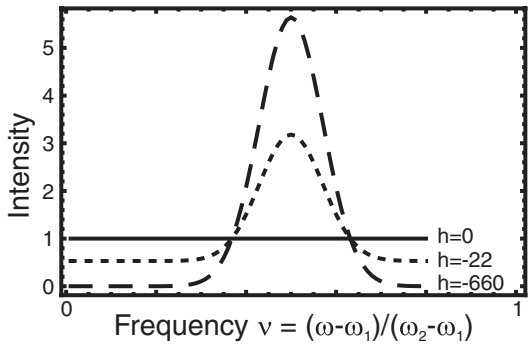

FIG. 2. Three simulated spectra with equal photon counts and their relative entropy (h) values. For a homogeneous spectrum (solid curve), the h is highest, whereas increasing spectral features lead to a progressively lower entropy (dashed curves). Since h denotes relative entropy, it is allowed to be negative.

all decaying resonances continue decaying, we can attempt to extend the autocorrelation with (non-zero) values that are consistent with the existing ones. Once these autocorrelation values are found, the corresponding intensity spectrum becomes a continuous function on the frequency interval that was measured. The MEM describes a method of finding autocorrelation values for $t > T_{max}$ by quantifying the information content of a spectrum by means of the spectral entropy h:

$$h = \int_0^1 \log[I(\nu)]\mathrm{d}\nu \tag{7}$$

with

$$\nu = \frac{\omega - \omega_1}{\omega_2 - \omega_1}, \tag{8}$$

a rescaled frequency whose value changes from 0 to 1 along the frequency interval $[\omega_1, \omega_2]$. The value of h provides a measure of the information content of a spectrum. An example is given in Fig. 2. Here, three spectra have been generated with an equal photon count. The least structured of these spectra has an entropy value of zero. The entropy value decreases when the spectrum becomes more structured, which indicates that the information content of the spectrum is higher. It should be noted that, unlike thermodynamic entropy, negative values for spectral entropy are allowed since h represents a relative value. Adding features, such as the ringing that is introduced when $R(t)$ is padded with zeros and transformed to the frequency domain, would further decrease the spectral entropy. We are therefore looking for the $R(t)$ that is consistent with the known data points and which has the highest possible entropy value (i.e., which adds no information to the spectrum).

Since $R(t)$ is known for values up to $t = T_{max}$, we can calculate $R(t)$ for $t > T_{max}$ by requiring that adding an additional autocorrelation point does not alter the spectral entropy, and therefore does not introduce any additional features in the intensity spectrum. The computational procedure is summarized in Fig. 1(f). The requirement of constant entropy can be satisfied by setting the derivative of the entropy with respect to the added autocorrelation point $R(m > M)$ equal to zero:

$$\frac{\mathrm{d}h}{dR(m > M)} = 0 = \int_0^1 \frac{1}{I(\nu)} \frac{\mathrm{d}I(\nu)}{\mathrm{d}R(m > M)}\mathrm{d}\nu. \tag{9}$$

Since spectrum and autocorrelation are related by the Fourier transform, the above formula requires that the Fourier transform of $1/I(\nu)$ is zero for $t > T_{max}$, while remaining consistent with $I(\nu)$ for $t \leq T_{max}$. The ability to retrieve a complex spectrum stems from the description of the intensity spectrum in terms of $1/I(\nu)$. Since this function is real and positive, we can introduce a complex valued function $g(\nu)$, so that

$$\frac{1}{I(\nu)} = |g(\nu)|^2. \tag{10}$$

The expression for $g(\nu)$ is not unique. Our spectrum, however, consists of a collection of exponentially decaying oscillations. According to Eq. (3), a resonance is described by the fraction $1/(\omega - \omega_{0,n} - i\Upsilon_n)$. Since ω is limited to real values, the denominator of this fraction will never be zero (unless Υ_n is zero). Mathematically speaking, we can postulate a complex frequency $\omega_c = \omega_{0,n} + i\Upsilon_n$, for which the denominator does vanish.

Because the Fourier components of $1/I(\nu)$ are zero for $m > M$, we can write $g(\nu)$ as a Fourier series $\sum a_m exp(im\nu)$ with $m \in \{0, 1, 2, \ldots, M\}$. This makes $g(\nu)$ effectively an order M polynomial, which has M zeroes at complex frequencies. The positions of these zeroes correspond to the position of resonances: since $g(\nu)$ is zero at these point, $I(\nu)$ is infinite. At such a point, the real value of ν corresponds to the resonance frequency. The imaginary part of the complex frequency determines the line width and whether the oscillation corresponding to the resonance is decaying ($\mathrm{Im}[\omega_c] = \Upsilon_n > 0$) or growing in time($\mathrm{Im}[\omega_c] = \Upsilon_n < 0$). Since only decaying resonances are allowed, we therefore have to find a solution for $g(\nu)$ for which all zeros occur at $\mathrm{Im}[\nu] > 0$.

Since both $g(\nu)$ and its complex conjugate are valid solutions for Eq. (10), every node of $g(\nu)$ can be freely exchanged by its complex conjugate. Thus, there are 2^M equivalent solutions, of which only a single solution consists of only decaying resonances. Burg showed[70] that the solution with only decaying resonances can be found by solving the matrix equation

$$\begin{pmatrix} R(0) & R^*(1) & \cdots & R^*(M) \\ R(1) & R(0) & \cdots & R^*(M-1) \\ \vdots & \vdots & \ddots & \vdots \\ R(M) & R(M-1) & \cdots & R(0) \end{pmatrix} \begin{pmatrix} 1 \\ a_1 \\ a_2 \\ \vdots \\ a_M \end{pmatrix} = \begin{pmatrix} b \\ 0 \\ 0 \\ \vdots \\ 0 \end{pmatrix} \tag{11}$$

for a_m and b. Here, b is a constant and a_m are Fourier coefficients, so that $g(\nu) \propto \sum a_m exp(im\nu)$. As a result, the complex $\boldsymbol{\chi}^{(2)}$ is given by

$$\chi^{(2)}(\nu) = \frac{e^{i\phi}}{g(\nu)} = \frac{be^{i\phi}}{1 + \sum_{m=1}^{M} a_m e^{im\nu}}. \tag{12}$$

The phase ϕ, a uniform phase factor, represents the last unknown in this analysis. The MEM algorithm described by Eq. (11) returns a complex-valued spectrum for which the relative phase (i.e., between different spectral points) is known. However, since $|\boldsymbol{\chi}^{(2)}|^2$ is identical to $|\boldsymbol{\chi}^{(2)}e^{i\phi}|^2$, the actual value of this phase is lost. Therefore, one must resort to

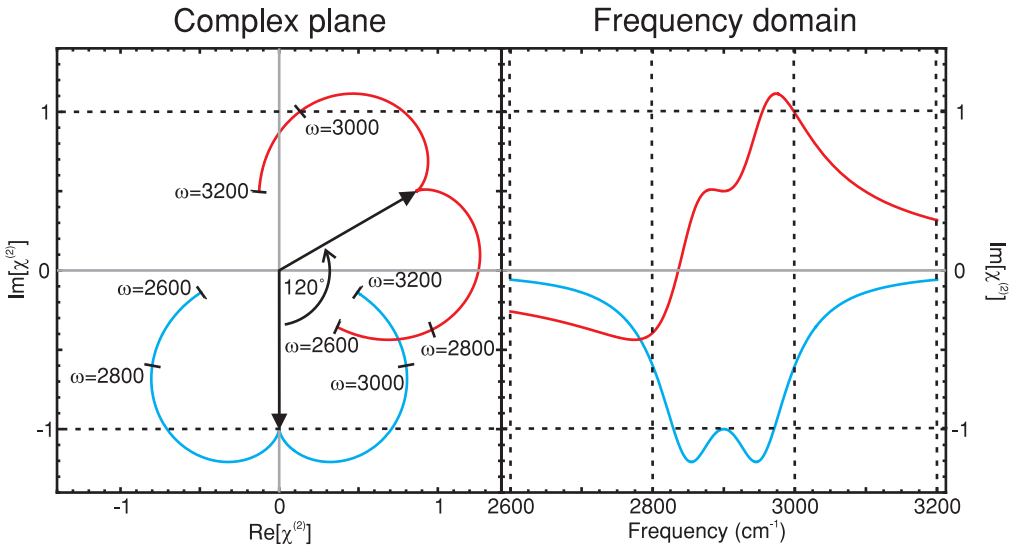

FIG. 3. Simulation of the effect of error phase on the shape of the Im$\chi^{(2)}$ spectrum. A spectrum consisting of resonances follow a curved pattern in the complex plane (left). The Im$\chi^{(2)}$ spectrum is the projection of this curve on the imaginary axis (right). An error phase rotates the complex curve around the origin. Shown here are the original spectrum (blue curve) and the same spectrum with an added (arbitrary) phase of 120° to simulate a possible outcome of MEM analysis (red curve). In the two cases, the imaginary spectra are radically different from each other. By rotating the complex curve around the origin and applying a suitable external criterion – in this case, requiring that all resonances point downward – the error phase can be eliminated.

additional criteria to obtain the correct absolute phase ϕ and thereby, the correct spectral shape of Im[$\chi^{(2)}$].

Figure 3 shows an illustration of the effect of the error phase on the outcome of the MEM reconstruction. Two cases are shown: the actual spectrum that is simulated and which should be recovered after applying the right error phase correction (blue curves), and a possible outcome of the MEM algorithm with an error phase still present (red curves). Here, we simulated an error phase of 120°, but in practical cases it is unknown. Figure 3 (left) shows the two spectra projected onto the complex plane, while Fig. 3 (right) shows the imaginary parts of the two spectra.

The simulated complex spectrum of a $\chi^{(2)}$ consisting of two resonances follows a curve in the complex plane [Fig. 3 (left, blue curve)]. In the frequency domain [Fig. 3 (right, blue curve)], Im[$\chi^{(2)}$] takes on the shape of a double Lorenzian resonance. Introducing an arbitrary error phase (in this case we have chosen 120°) rotates this curve around the origin by the same amount [Fig. 3 (left, red curve)], so that the equivalent curve in the frequency domain [Fig. 3 (right, red curve)] takes on a derivative line shape.

In practice, we have to recover the blue curve in Fig. 3 by multiplying the complex values of the red curve of Fig. 3 with a complex value $e^{i\phi}$. To this end, we have to set a suitable criterion (see also the supporting information accompanying Ref. 34). In this example, we required that (1) the imaginary part has a Lorentzian shape for all resonances and (2) the imaginary part of all resonances is purely negative. Finding the value of ϕ that corresponds most closely to these criteria (in this example $\phi = -120°$) will then recover the blue curves of Fig. 3.

It should be noted that the error phase correction does not alter the relative phase of individual spectral points with respect to each other. Therefore, even without error phase correction a relation can be established, for instance the phase difference between a non-resonant background and resonant peaks.[71]

III. RESULTS AND DISCUSSION

A. Comparison of PS-SFG with MEM analysis

Although recent results obtained by MEM analysis have been tested against phase sensitive SFG measurements (e.g., the experimental results of Ref. 34 have been compared[44] with those of Mondal *et al.*[41] and the computational results of Nagata and Mukamel[43]), no direct comparison of the same spectrum by two different methodologies – MEM and PS-SFG – exists up to date. In this section we investigate to what extent MEM predicts the correct complex $\chi^{(2)}$ and how possible discrepancies can be explained. To this end, we have analyzed previously published[35] PS-SFG data, for which both Im[$\chi^{(2)}$] and $|\chi^{(2)}|^2$ are known, and feed the $|\chi^{(2)}|^2$ into a MEM algorithm. We then analyze the extent to which complex $\chi^{(2)}$ spectra obtained from PS-SFG and MEM are similar, given a perfect value for the error phase, and what influence an incorrect choice for the error phase has on the results in the MEM case.

Several recent studies have reported on the structure of the neat water/vapor interface and that of the water/DPPC interface by means of phase-sensitive SFG. Here we have reproduced spectra reported by Chen *et al.*[35] Figures 4(a) and 4(d) show the $|\chi^{(2)}|^2$ response of the water/DPPC and the neat water/vapor interface, respectively. Both spectra show bands that are characteristic for water centered at ~3200 and ~3400 cm^{-1}. Further information on this band structure can be obtained by considering phase-sensitive information. Figures 4(b) and 4(e) show the real (gray curve) and imaginary part (black curve) of the susceptibility $\chi^{(2)}$. In the case of the water/DPPC interface (Fig. 4(b)), both water bands

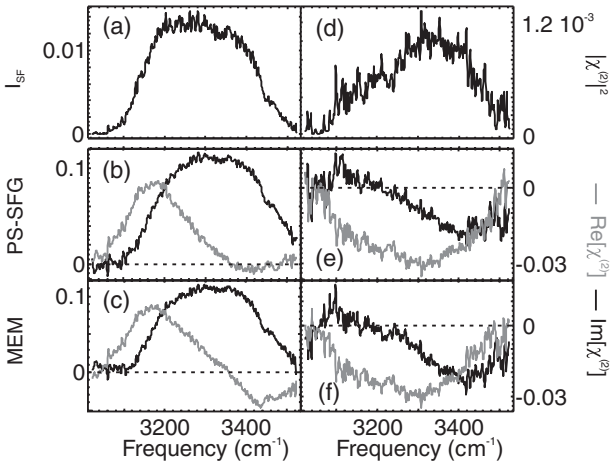

FIG. 4. Comparison of phase-sensitive SFG measurements with maximum entropy phase retrieval for a water-DPPC (a)–(c) and a water-vapor (d)–(f) interface. Shown are absolute square (a) and (d) of $\chi^{(2)}$ as well as the real (gray) and imaginary (black) parts of $\chi^{(2)}$ obtained from phase-sensitive measurements (b and e) and the MEM algorithm (c and f). Intensity and amplitude units are given relative to the z-cut quartz reference.

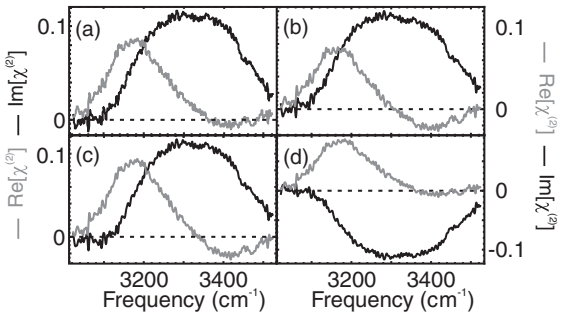

FIG. 5. Simulation of distortions induced by experimental or computational effects: (a) undistorted PS-SFG spectrum from Fig. 4(b), (b) distortion induced by a phase shift of 10°, (c) distortion induced by a phase drift of exp [$i\omega t$] of 40 fs, and (d) complex conjugation of the spectrum.

interfere constructively, while for the water/vapor interface (Fig. 4(e)) the change of sign of Im[$\chi^{(2)}$] at 3200 cm^{-1} suggests a destructive interference between the two bands.

The above phase sensitive measurements were used as a test case for our MEM phase retrieval algorithm. By feeding the $|\chi^{(2)}|^2$ spectrum of Figs. 4(a) and 4(d) into the MEM algorithm, we obtain a complex spectrum of which the complex $\chi^{(2)}$ should, theoretically, resemble the spectra of Figs. 4(b) and 4(e) up to a phase factor corresponding to the error phase. Therefore, by choosing an appropriate phase correction, it should be possible to obtain a spectrum with close correspondence to Figs. 4(b) and 4(e).

Finally, Figs. 4(c) and 4(f) show the complex spectra obtained from MEM analysis of the intensity spectra of Figs. 4(a) and 4(b), respectively. For both datasets, Im[$\chi^{(2)}$] closely resembles the Im[$\chi^{(2)}$] obtained in phase-sensitive analysis. The change of sign of Im[$\chi^{(2)}$] at 3200 cm^{-1} of the spectrum of the water/vapor interface, for instance, is reproduced in the MEM analysis. A difference can be observed for the real part of $\chi^{(2)}$. The difference is most clear for the water/DPPC interface, where for the phase sensitive measurement [Fig. 4(b)] Re[$\chi^{(2)}$] remain near zero in the spectral region between 3400–3500 cm^{-1}, whereas the MEM analysis [Fig. 4(c)] predicts a negative value for Re[$\chi^{(2)}$].

B. Possible sources of error

Our analysis shows that PS-SFG and MEM analysis can arrive at the same complex spectrum for a given sample. This result, however, is not guaranteed, since experimental and computational circumstances may lead to deviations or artifacts. Figure 5 shows a simulation of the different distortions that may occur due to experimental or computational effects. Figure 5(a) shows the same PS-SFG spectrum as Fig. 4(b). Several experimental or computational effects may lead to distortions of this spectrum, which may explain the discrepancy between the PS-SFG spectrum of Fig. 4(b) and the MEM analysis of Fig. 4(c).

1. Phase shift

Figure 5(b) shows the effect of a uniform phase shift of 10°. Such a phase shift is most likely to occur when the phase of the reference is away from its assumed value. In a PS-SFG experiment, the reference is external, i.e., a separate sample is used as reference. The reference sample in a PS-SFG experiment should be far from resonance for all wavelengths involved. In such cases, it is reasonable to assume that the nonlinear susceptibility of the reference is purely real, so that this phase can be taken as a zero point. In most PS-SFG experiments, a quartz crystal is used as reference. We were unable to obtain quartz phase information for wavelength >2 μm. When the susceptibility of the reference sample is not purely real, e.g., when the reference sample is on or close to resonance, then the assumption of a zero phase leads to an incorrect reconstruction of the complex spectrum.

For the MEM the reference is internal, i.e., the overall phase is set by making an assumption on a feature in the spectrum (the shape of a peak or the phase of a background). Therefore, any phase shift in a PS-SFG experiment will be systematic, while phase shifts in a MEM reconstruction can be expected to show more variation. A uniform phase shift can be corrected for using the same procedure as the MEM error phase correction. We will list suitable criteria for error phase correction in Sec. III C, which can be applied to both PS-SFG and MEM complex spectra.

2. Phase drift

PS-SFG requires a stable experimental configuration. Care should be taken that the time delay T between the signals of the local oscillator and the sample or reference does not change between measurements. A difference in time delay would lead to a phase modulation exp [$i\omega\Delta T$], where ΔT is the time delay difference. For typical bandwidths of broadband systems, ω varies over a range of 250–400 cm^{-1}, so that a difference in time delay of 40 fs leads to a phase drift of 17°–27° over the range of the spectrum. The effect of such a phase drift can be seen in Fig. 5(c): in this case, the peak in

Re[$\chi^{(2)}$] at 3200 cm^{-1} is enhanced, while the dip below zero at 3400 cm^{-1} is more pronounced compared to Fig. 5(a).

3. Complex conjugation

It is important to note an ambiguity exists in representing complex spectra for both MEM and PS-SFG. In Eq. (3) we assumed a (decaying) resonance $\exp(i\omega t - \Upsilon t)$. Since the sign choice of $i\omega t$ is arbitrary – for an electromagnetic wave we can equally well write $(-i\omega t)$ – both Eq. (3) and its complex conjugate are adequate descriptions of the resonance spectrum. As a result, we have to choose a sign convention to use for the sign in front of $i\Upsilon_n$ in Eq. (3) (in our case minus). Figure 5(d) shows the effect of complex conjugation of a spectrum: changing the sign of $i\Upsilon_n$ changes the sign of Im[$\chi^{(2)}$]. It is therefore important to ensure sign conventions have been applied consistently.

The choice of sign is implicitly present in the computational procedures for both PS-SFG and MEM analysis: a sign change alters the relation between spectrum and autocorrelation from a (forward) Fourier transform to an inverse Fourier transform and leads to two possible solutions for the complex spectrum that are each others complex conjugate. Alternatively, complex conjugation of the spectrum is also realized by reversing data order[44] (from increasing wavelength to decreasing wavelength order) or by reversing the step filter in the time domain: the filter of Figs. 1(c) or 1(d) can be reversed, so that either the left lobe (PS-SFG) or left half (MEM) of the autocorrelation is used. The resulting spectrum is again complex conjugated with respect to the regular result. Since complex conjugation cannot be corrected for by applying a phase factor, such as in the error phase correction procedure, care must be taken that the same conventions are used when comparing spectra.

4. Other causes

For a successful MEM analysis, a spectral recording is needed that is as clean as possible. Any background signal must be subtracted and all intensities must be corrected for excitation intensity, preferably by dividing with a reference intensity signal. Since the entropy is given by the logarithm of intensity, care should be taken that all intensity values are larger than zero. Due to the nonlinear nature of the MEM analysis process, it is not possible to establish a direct relation between disturbances in source data and their influence on MEM analysis results. It remains advisable, therefore, to test the robustness of a MEM reconstruction by artificial variation of such corrections.

C. Error phase correction

An error phase correction will always be required for MEM and might be required for PS-SFG. In order to find the most accurate correction, one of the following criteria can be used:

(1) In the presence of sharp resonances (e.g., C–H or S–O resonances), we can use the property that the imaginary part of these resonances is either purely positive or purely negative and follows a line shape that is symmetric, which may be a Lorentzian, a Gaussian, or a Voigt profile.[58,59] A deviation from a symmetric shape (e.g., such as the ones observed by Ji *et al.*[46]) is a strong indication a phase shift is still present. Also, when the nature of a resonant mode is known *a priori* this may be applied as an additional constraint for the phase shift correction. For example, in the case of a surface-grafted self-assembled monolayer, the grafted molecules will point away from the support. The sign of the complex resonance can therefore be constrained to the expected value.

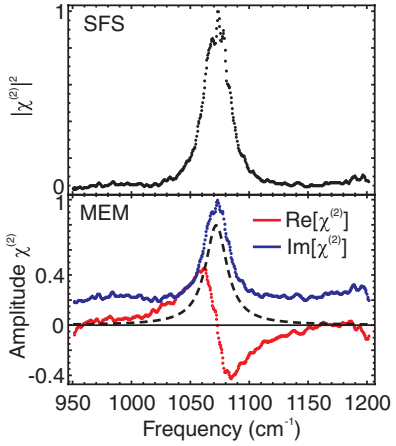

FIG. 6. Demonstration of a MEM reconstruction using external criteria. The top panel shows the sum frequency scattering spectrum of a 1% (v/v) oil-in-water emulsion in the presence of 8 mM SDS in the frequency range 950–1200 cm^{-1}. The bottom panel shows the MEM analysis of this intensity spectrum. Here, an error phase correction has been chosen so that the SO-stretch resonance shows a purely absorptive line shape in the imaginary while showing a derivative line shape in the real part of the amplitude spectrum. The black, dashed curve shows a single Lorentzian peak as a guide to the eye. Intensity and amplitude units are arbitrary.

(2) In the absence of isolated resonances, the presence of a non-resonant background may be exploited to obtain an estimate for the phase shift,[32,71] by requiring that the non-resonant signal does not contribute to the imaginary part of $\boldsymbol{\chi}^{(2)}$ or $\boldsymbol{\Gamma}^{(2)}$.

Figure 6 shows an example of a spectrum reconstructed with the first criterion. A sum frequency scattering signal was recorded from a 1% (v/v) hexadecane-in-water emulsion containing 8 mM sodium dodecyl sulfate (SDS). The spectrum was recorded in the 950–1200 cm^{-1} frequency region, which shows a single peak at 1070 cm^{-1}, commonly assigned to the sulfate symmetric stretch resonance. The bottom panel shows the MEM reconstruction of this spectrum. Here, we have taken the outcome of the MEM algorithm, and multiplied the complex value of every data point by the same phase factor $\exp[i\phi]$. ϕ was chosen such that the single peak at 1070 cm^{-1} is purely positive and symmetric for the imaginary spectrum (bottom panel). As a result, the real part of the complex spectrum shows a dispersive shape and a broadband background feature is visible, predominantly in the imaginary spectrum.

IV. CONCLUSION

We have shown the similarities between PS-SFG and phase reconstruction using the MEM algorithm. We show that

MEM can recover the complex spectrum underlying an non-interferometric recording when we assume that (1) all information is contained within the spectrum (i.e., the spectrum is described by a collection of resonances within the recorded frequency window and a non-resonant background) and (2) all resonances are the result of exponentially decaying oscillations. In a direct comparison of PS-SFG water spectra and their MEM-reconstructed counterpart, we have shown that MEM analysis does indeed yield a complex spectrum that follows the result from PS-SFG spectroscopy closely. We have analyzed the possible causes for discrepancies between MEM and PS-SFG, such as a shift or drift in the complex phase and complex conjugation. We show that these effects may both originate from numerical effects in MEM analysis as well as experimentally induced effects from PS-SFG. PS-SFG offers the advantage of an absolute phase detection, provided a suitable reference sample is used. The MEM, on the other hand, does not require a reference sample, a convenience that comes at the cost of having to correct for an error phase. This error phase must be corrected by means of some external criterion, for which we have discussed two possible methods. MEM can be applied to any SFG measurement and does not require a PS-SFG setup. MEM is especially valuable in cases where phase-sensitive modifications to the detection scheme are not possible, such as in the case of SF scattering[33,60,64,65] or SF microscopy.[72,73]

V. EXPERIMENTAL DETAILS

A. PS-SFG experiments

PS-SFG measurements were performed using the setup described here, which is based upon the design by Nihonyanagi *et al.*[39] A 300 μJ visible (VIS) (2 ps, 792 nm, s-polarized) and a 10 μJ infrared (IR) beam (85 fs, p-polarized, centered at 3250 cm^{-1}) are spatially and temporally overlapped at incident angles of 50° and 60° on a first stage, which contains either a sample or a z-cut quartz surface as reference. The reflected IR, VIS, and SF pulses were then refocused with a gold concave mirror (f = 100 mm) onto a second stage containing a GaAs crystal surface (Lambda Precision Optics), which functions as LO and generates a second SFG signal. The SFG signal from the first stage was delayed by 2.5 ps by passing it through a 1 mm thick silica plate positioned before the mirror. The interference spectrum resulting from the two SFG signals was spectrally dispersed (Acton Research, SpectraPro SP-500 monochromator with a 1200 g/mm grating blazed at 750 nm) and then detected by a liquid nitrogen cooled charge-coupled device (CCD) (Roper Scientific, 1340 × 400 pixel array, LN400EB back illuminated CCD).

1,2-Dipalmitoyl-sn-glycero-3-phosphocholine (DPPC) was purchased from Avanti Polar Lipids (Alabaster, AL). Spectrophotometric grade chloroform and methanol were purchased from Fisher Scientific and used as a mixed solvent for spreading of the phospholipids. The concentration of phospholipid stock solutions was ≈1 mM.

The neat water/vapor and water/DPPC interfaces were prepared using Nanopure water in Petri-dishes (5 cm diameter). Nanopure water (not purged of CO_2) with a resistivity of 18.2–18.3 MΩ cm and a measured pH of 5.5 was from a Barnstead Nanopure system (model D4741) with additional organic removing cartridges (D5026 Type I ORGANICfree Cartridge Kit; Pretreat Feed). DPPC monolayers were overspread (≈10 μl) on neat water. After spreading, 10 min was allowed for solvent evaporation and monolayer stabilization to equilibrium spreading pressure before PS-SFG measurements were conducted. Under this condition, monolayers were equilibrated in the liquid condensed (LC) phase, which corresponds to a highly ordered monolayer on the water surface.

B. Sum frequency scattering experiments

Sum frequency scattering measurements were performed with the laser system described in Ref. 74: a 10 μJ IR pulse (150 fs, centered around 1100 cm^{-1}, FWHM bandwidth >140 cm^{-1} and a 10 μJ VIS pulse (800 nm, FWHM bandwidth 12 cm^{-1}) were spatially and temporally overlapped in a CaF_2 cuvette with an optical path length of 0.1 mm. The infrared and visible pulses were incident in the horizontal plane under a relative angle of 15°. The infrared pulse was polarized in the horizontal direction, while the visible pulse was polarized in the vertical direction. Scattered SF light was captured in the same plane at a scattering angle of 60°, around a solid angle of 20°, selected for vertical polarization, and spectrally dispersed onto an intensified CCD camera (I-STAR, Andor Technologies).

Emulsion samples were prepared using the method described by de Aguiar *et al.*[65] 2 vol.% of hexadecane (≥99.9%, Fluka) was mixed with a D_2O (>99%, Sigma-Aldrich) solution containing 100 μmol purified SDS (>99%, Alpha Aesar) in a 5 ml vial using an OMNI TIP homogenizer. The resultant mixture was treated in an ultrasonic bath for 15 min and further diluted with a solution of SDS in D_2O so that the final emulsion contained 1% (v/v) hexadecane in water at an SDS concentration of 8 mM.

ACKNOWLEDGMENTS

This work is part of the research program of the Max Planck Society. Additional funding was received from NSF-CHE, the German Science Foundation (DFG) under Contract No. 560398 and the European Research Council (ERC) under Contract No. 240556. We have prepared an interactive phase reconstruction program based on the MEM algorithm, which is available at http://lbp.epfl.ch/.

[1] Y. R. Shen, Nature (London) **337**, 519 (1989).
[2] T. F. Heinz, "Second-order nonlinear optical effects at surfaces and interfaces," in *Nonlinear Surface Electromagnetic Phenomena* (Elsevier, New York, 1991), Chap. 5, p. 353.
[3] J. F. McGilp, J. Phys.: Condens. Matter **2**, 7985 (1990).
[4] Y. R. Shen, Surf. Sci. **299/300**, 551 (1994).
[5] C. D. Bain, J. Chem. Soc., Faraday Trans. **91**, 1281 (1995).
[6] K. B. Eisenthal, Chem. Rev. **96**, 1343 (1996).
[7] N. Bloembergen, Appl. Phys. B **68**, 289 (1999).
[8] M. J. Shultz, C. Schnitzer, D. Simonelli, and S. Baldelli, Int. Rev. Phys. Chem. **19**, 123 (2000).
[9] G. L. Richmond, Annu. Rev. Phys. Chem. **52**, 357 (2001).

[10]M. J. Schultz, C. Schnitzer, D. Simonelli, and S. Baldelli, J. Phys. Chem. B **106**, 5313 (2002).
[11]Z. Chen, Y. R. Shen, and G. A. Somorjai, Annu. Rev. Phys. Chem. **53**, 437 (2002).
[12]G. L. Richmond, Chem. Rev. **102**, 2693 (2002).
[13]S. Sioncke, T. Verbiest, and A. Persoons, Mater. Sci. Eng. R. **42**, 115 (2003).
[14]G. J. Simpson, ChemPhysChem. **5**, 1301 (2004).
[15]M. B. Raschke and Y. R. Shen, Curr. Opin. Solid State Mater. Sci **8**, 343 (2004).
[16]M. A. Belkin and Y. R. Shen, Int. Rev. Phys. Chem. **24**, 257 (2005).
[17]A. G. Lambert, P. B. Davies, and D. J. Neivandt, Appl. Spectrosc. Rev. **40**, 103 (2005).
[18]F. Vidal and A. Tadjeddine, Rep. Prog. Phys. **68**, 1095 (2005).
[19]Q. Du, R. Superfine, E. Freysz, and Y. R. Shen, Phys. Rev. Lett. **70**, 2313 (1993).
[20]D. E. Gragson and G. L. Richmond, J. Phys. Chem. B **102**, 3847 (1998).
[21]A. V. Benderskii, J. Henzie, S. Basu, X. M. Shang, and K. B. Eisenthal, J. Phys. Chem. B **108**, 14017 (2004).
[22]Y. R. Shen and V. Ostroverkhov, Chem. Rev. **106**, 1140 (2006).
[23]S. Gopalakrishnan, D. F. Liu, H. C. Allen, M. Kuo, and M. J. Shultz, Chem. Rev. **106**, 1155 (2006).
[24]W. Gan, D. Wu, Z. Zhang, R. R. Feng, and H. F. Wang, J. Chem. Phys. **124** (2006).
[25]J. Kim, G. Kim, and P. S. Cremer, Langmuir **17**, 7255 (2001).
[26]S. Roke, J. Schins, M. Muller, and M. Bonn, Phys. Rev. Lett. **90** (2003).
[27]M. R. Watry, T. L. Tarbuck, and G. I. Richmond, J. Phys. Chem. B **107**, 512 (2003).
[28]H. Chen, W. Gan, R. Lu, Y. Guo, and H. F. Wang, J. Phys. Chem. B **109**, 8064 (2005).
[29]G. Ma and H. C. Allen, Langmuir **22**, 11267 (2006).
[30]C. M. Johnson, A. B. Sugiharto, and S. Roke, Chem. Phys. Lett. **449**, 191 (2007).
[31]M. Sovago, G. W. H. Wurpel, M. Smits, M. Muller, and M. Bonn, J. Am. Chem. Soc. **129**, 11079 (2007).
[32]M. Sovago, E. Vartiainen, and M. Bonn, J. Phys. Chem. C **113**, 6100 (2009a).
[33]S. Roke, ChemPhysChem. **10**, 1380 (2009).
[34]M. Sovago, E. Vartiainen, and M. Bonn, J. Chem. Phys. **131** (2009).
[35]X. Chen, W. Hua, Z. Huang, and H. C. Allen, J. Am. Chem. Soc. **132**, 11336 (2010).
[36]N. Ji, V. Ostroverkhov, C. S. Tian, and Y. R. Shen, Phys. Rev. Lett. **100**, 096102 (2008).
[37]M. Sovago, R. K. Campen, G. W. H. Wurpel, M. Muller, H. J. Bakker, and M. Bonn, Phys. Rev. Lett. **101** (2008).
[38]Y. B. Fan, X. Chen, L. J. Yang, P. S. Cremer, and Y. Q. Gao, J. Phys. Chem. B **113**, 11672 (2009).
[39]S. Nihonyanagi, S. Yamaguchi, and T. Tahara, J. Chem. Phys. **130**, 204704 (2009).
[40]S. Nihonyanagi, S. Yamaguchi, and T. Tahara, J. Am. Chem. Soc. **132**, 6867 (2010).
[41]J. A. Mondal, S. Nihonyanagi, S. Yamaguchi, and T. Tahara, J. Am. Chem. Soc. **132**, 10656 (2010).
[42]G. Ma, X. K. Chen, and H. C. Allen, J. Am. Chem. Soc. **129**, 14053 (2007).
[43]Y. Nagata and S. Mukamel, J. Am. Chem. Soc. **132**, 6434 (2010).
[44]M. Sovago, E. Vartiainen, and M. Bonn, J. Chem. Phys. **133**, 229901 (2010).
[45]V. Ostroverkhov, G. A. Waychunas, and Y. R. Shen, Phys. Rev. Lett. **94** (2005).
[46]N. Ji, V. Ostroverkhov, C. Y. Chen, and Y. R. Shen, J. Am. Chem. Soc. **129**, 10056 (2007).
[47]C. S. Tian and Y. R. Shen, J. Am. Chem. Soc. **131**, 2790 (2009).
[48]X. K. Chen and H. C. Allen, J. Phys. Chem. B **114**, 14983 (2010).
[49]S. Haykin and S. Kesler, in *Prediction-Error Filtering and Maximum-Entropy Spectral Estimation* (Springer-Verlag, Berlin, 1983), Chap. 2, pp. 9–70.
[50]J. F. Ehlers, *MESA and Trading Market Cycles* (Wiley, New York, 2002).
[51]S. Sibisi, J. Skilling, R. G. Brereton, E. D. Laue, and J. Staunton, Nature (London) **311**, 446 (1984).
[52]W. Dong, T. Baird, J. R. Fryer, C. J. Gilmore, D. D. Macnicol, G. Bricogne, D. J. Smith, M. A. Okeefe, and S. Hovmoller, Nature (London) **355**, 605 (1992).
[53]R. Kitaura, S. Kitagawa, Y. Kubota, T. C. Kobayashi, K. Kindo, Y. Mita, A. Matsuo, M. Kobayashi, H.-C. Chang, T. C. Ozawa, M. Suzuki, M. Sakata, and M. Takata, Science **298**, 2358 (2002).
[54]E. M. Vartiainen, K. E. Peiponen, H. Kishida, and T. Koda, J. Opt. Soc. Am. B **13**, 2106 (1996).
[55]E. M. Vartiainen, J. Opt. Soc. Am. B **9**, 1209 (1992).
[56]E. M. Vartiainen, H. A. Rinia, M. Muller, and M. Bonn, Opt. Express **14**, 3622 (2006).
[57]H. A. Rinia, M. Bonn, M. Muller, and E. M. Vartiainen, ChemPhysChem **8**, 279 (2007).
[58]P. K. Yang and J. Y. Huang, J. Opt. Soc. Am. B **14**, 2443 (1997).
[59]P. K. Yang and J. Y. Huang, J. Opt. Soc. Am. B **17**, 1216 (2000).
[60]S. Roke, W. G. Roeterdink, J. E. G. J. Wijnhoven, A. V. Petukhov, A. W. Kleyn, and M. Bonn, Phys. Rev. Lett. **91**, 258302 (2003).
[61]S. Roke, J. Buitenhuis, J. C. van Miltenburg, M. Bonn, and A. van Blaaderen, J. Phys. Condens. Matter **17**, S3469 (2005).
[62]S. Roke, O. Berg, J. Buitenhuis, A. van Blaaderen, and M. Bonn, Proc. Natl. Acad. Sci. U.S.A **103**, 13310 (2006).
[63]A. G. F. de Beer and S. Roke, Phys. Rev. B **75**, 245438 (2007).
[64]A. G. F. de Beer, H. B. de Aguiar, J. F. W. Nijsen, and S. Roke, Phys. Rev. Lett. **102**, 095502 (2009).
[65]H. B. de Aguiar, A. G. F. de Beer, M. L. Strader, and S. Roke, J. Am. Chem. Soc. **132**, 2122 (2010).
[66]A. G. F. de Beer and S. Roke, J. Chem. Phys. **132**, 234702 (2010).
[67]M. L. Strader, H. B. de Aguiar, A. G. F. de Beer, and S. Roke, Soft Matter **7**, 4959 (2011).
[68]H. B. de Aguiar, M. L. Strader, A. G. F. de Beer, and S. Roke, J. Phys. Chem. B **115**, 2970 (2011).
[69]S. Roke, M. Bonn, and A. V. Petukhov, Phys. Rev. B **70**, 115106 (2004).
[70]J. P. Burg, Ph.D. dissertation, Stanford University 1975.
[71]R. Vacha, S. Rick, P. Jungwirth, A. G. F. de Beer, H. B. de Aguiar, J.-S. Samson, and S. Roke, J. Am. Chem. Soc. **133**, 10204 (2011).
[72]K. Cimatu and S. Baldelli, J. Am. Chem. Soc. **128**, 16016 (2006).
[73]K. A. Cimatu and S. Baldelli, J. Phys. Chem. C **113**, 16575 (2009).
[74]A. B. Sugiharto, C. M. Johnson, H. B. de Aguiar, L. Alloatti, and S. Roke, Appl. Phys. B **91**, 315 (2008).